Journal Name

ARTICLE

Transition metal complexes of a versatile polyalkoxy oxazolidine-based ligand derived from *in-situ* cyclization

Received 00th January 20xx,
Accepted 00th January 20xx

DOI: 10.1039/x0xx00000x

www.rsc.org/

Ayaan Saleem,[a] Paulina A. Kobielska,[a] Klaus Harms,[b] Maria G. Katsikogianni,[a] Richard Telford,[a] Ghenadie Novitchi[c] , and Sanjit Nayak*[a]

One-pot reaction between 8-hydroxyquinoline-2-carboxaldehyde (HQC) and tris(hydroxymethyl)aminomethane (TRIS) followed by *in situ* cyclization yielded an oxazolidine based ligand which produced four mononuclear complexes of Mn^{II}(**1**), Co^{II}(**2**), Ni^{II}(**3**), Zn^{II}(**4**), a tetranuclear iron (Fe^{III}_4) complex (**5**) and a trinuclear cobalt ($Co^{II}Co^{III}_2$) complex (**6**). Magnetic studies show dominant antiferromagnetic interaction in tetranuclear iron (Fe^{III}_4) complex (**5**) and presence of the slow relaxation of magnetisation in **6** . The compounds were also studied for their antibacterial properties. The oxazolidine ligand (H_3L_2) of this study showed good antimicrobial activity not only against Gram-positive bacteria but also against Gram-negative bacteria. The antimicrobial efficacy of metal complexes (**1**-**6**) is also reported.

Introduction

Synthesis of polynuclear transition metal complexes has gained much attention in recent years due to their promising applications in single-molecule magnets (SMMs), quantum computing, and biomimetic catalysis.[1-4] Use of polyalkoxy ligands is a widely accepted strategy to synthesize polynuclear coordination complexes.[5-11] One of the popular ways to design new polyalkoxy ligands is through Schiff-base condensation between hydroxyaldehydes and aminoalcohols.[12-23] In line with our interest in designing new polynuclear coordination complexes for studying magnetic and biomimetic properties, we coupled 8-hydroxyquinoline and tris(hydroxymethyl)aminomethane to design the desired Schiff-base ligand H_4L_1 (Scheme 1). However, the reaction between 8-hydroxyquinoline-2-carboxaldehyde (HQC) and tris(hydroxymethyl)aminomethane (TRIS) yielded an oxazolidine derivative by *in situ* cyclization, and produces H_3L_2 during the synthesis. Conventionally oxazolidines can be synthesized by condensation of β-hydroxylamine and carbonyl compounds with loss of one molecule of water followed by a cyclization step.[24] Oxazolidines are also synthesized by the reaction of aziridines with carbonyl compounds.[25] Oxazolidines are well known for their interesting properties and widely used in asymmetric synthesis as chiral auxiliaries and has pharmacological applications due to their antimicrobial and anti epileptic properties. [24, 26-31] Use of oxazolidines as ligands have been observed in literature in past particularly for developing asymmetric catalysts. [32-34] 8-hydroxyquinoline-2-carboxaldehyde has been recently used with a range of amines to synthesize lanthanide based Schiff-base complexes. [35, 36] Here we are reporting six new complexes of H_3L_2 with different transition metals, including three isostructural mononuclear six-coordinate complexes of Mn^{II}(**1**), Co^{II}(**2**), Ni^{II}(**3**), one mononuclear five-coordinate complex of Zn^{II}(**4**), a tetranuclear iron (Fe^{III}_4) complex (**5**) and a trinuclear cobalt ($Co^{II}Co^{III}_2$)

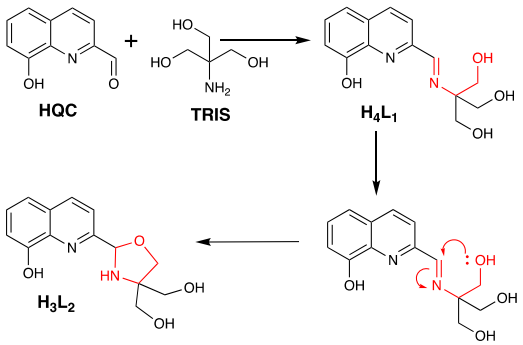

Scheme 1. Synthetic scheme of the desired ligand (H_4L_1) and the produced oxazolidine (H_3L_2) is shown with the proposed mechanism.

[a] *School of Chemistry and Biosciences, Faculty of Life Sciences, University of Bradford, Richmond Road, Bradford, West Yorkshire, BD7 1DP, United Kingdom.*
[b] *Universitaet Marburg, Fachbereich Chemie, Hans-Meerwein-Str. 4, 35032 Marburg, Germany*
[c] *Laboratoire National des Champs Magnétiques Intenses, CNRS UPR 3228, 25 Rue des Martyrs, 38042, Grenoble, France*
† Footnotes relating to the title and/or authors should appear here.
Electronic Supplementary Information (ESI) available: Images of intermolecular hydrogen bonding networks and packing diagram, spectra (IR, NMR, ESI-MS), TGA, Arrhenius plot, crystallographic bond lengths and angles are available. See DOI: 10.1039/x0xx00000x

complex (**6**). All the complexes were characterized by single-crystal X-ray diffraction, in combination with infrared (IR) spectroscopy, electrospray ionization mass spectroscopy (ESI-MS), nuclear magnetic resonance (NMR) spectroscopy, thermogravimetric analyses (TGA), and elemental analyses. Antimicrobial activity of the complexes was tested against both gram-positive and gram-negative bacteria. Magnetic studies of the polynuclear complexes revealed that Compound **6** shows frequency dependent slow relaxation of magnetism at 2.5 K suggesting possible single-molecule magnet (SMM) behaviour.

Experimental

Materials and methods:

8-Hydroxyquinoline-2-carboxaldehyde was purchased from Acros Organics and all the other chemicals were purchased from Sigma Aldrich and used without any further purification. All the solvents were purchased from Fisher Scientific and used as received.

Elemental analyses (for C, H, and N) were carried out on a Perkin-Elmer 2400 series II analyzer. Fourier-transformed Infrared (FTIR) spectra were recorded over the range of 600-4000 cm^{-1} using Perkin-Elmer Spectrum 100 FTIR spectrometer fitted with a Perkin-Elmer Universal ATR sampling device. Thermogravimetric analyses (TGA) were carried out using TAQ5000IR Thermogravimetric analyser (TA instrument). Nitrogen purging gas flow of 10 mL min^{-1} and 5 °C min^{-1} heating ramp were used. A sample mass of approximately 5 mg was used and TA Instruments Universal Analysis 2000 software was employed to analyse the data. Electrospray ionization Mass Spectra (ESI-MS) were recorded using a Micromass Quattro Ultima Mass Spectrometer equipped with an electrospray ionization source, with a sample dissolved in methanol and injected at 10 µL/min.

X-ray crystallography: Except for Compound **5** all data were collected with a Bruker D8 QUEST area detector diffractometer equipped with with MoK_α radiation, a graded multilayer mirror monochromator (= 0.71073 Å) and a PHOTON-100 CMOS detector using an oil-coated shock-cooled crystal at 100(2) K. For Compound **5** data was collected with a Bruker APEX2 diffractometer equipped with CuK_α radiation, a graphite monochromator (= 1.54184 Å) and an APEX2 detector using an oil-coated shock-cooled crystal at 173(2) K. A multi-scan correction for absorption was applied using the program SADABS (Bruker AXS Inc., 2016). The structure was solved by direct methods by using the program XT V2014/1 (Bruker AXS Inc., 2014) and refined by full matrix least squares procedures on F^2 using SHELXL-2018/1 (Sheldrick, 2018).[37] More details on X-ray data collection of each compound is provided at the Electronic Supplementary Information (ESI).

NMR studies: Sample for H_3L_2 and Compound **4** were prepared in MeOD and in DMSO-d_6 (Goss Scientific, UK), respectively, at concentrations of 15 mg/mL before transferred to field matched 5 mm NMR tubes (Wilmad, USA). ^1H and ^{13}C NMR spectra were acquired at 303 K on a Bruker AVIII 400 MHz spectrometer equipped with a 5 mm SMART probe operating at 400.153 and 100.629 MHz for ^1H and ^{13}C respectively. $^1H^1H$-COSY and $^1H^{13}C$-HMBC spectra were collected in addition to the 1D data on Compound **4**. Spectra were phased, referenced to the residual solvent signal and processed using TopSpin v. 3.5pl7.

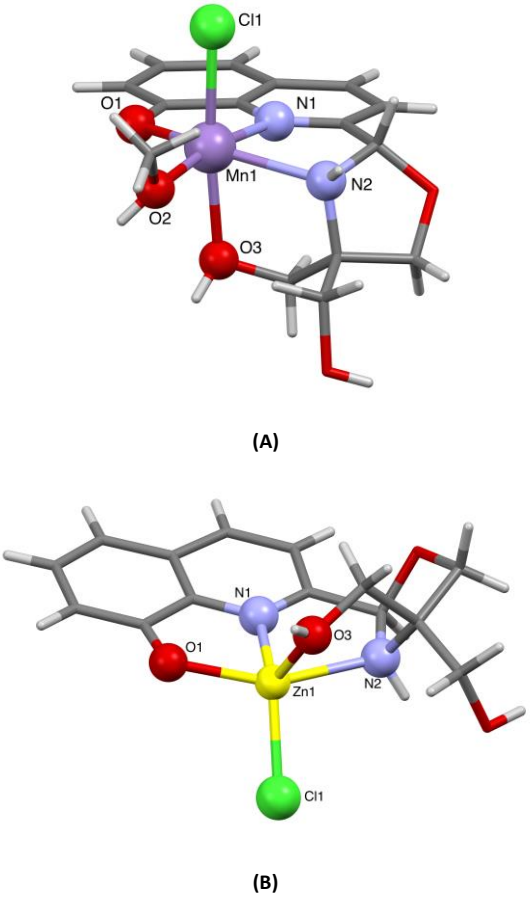

Figure 1. The structure of Compound **1** (A) and Compound **4** (B) as determined by X-ray crystallography are shown. Colour code for the atoms: Blue (N), grey (C), red (O), purple (Mn), and yellow (Zn).

Magnetic Studies: *Dc* magnetic susceptibility data (2-300 K) were collected on powdered samples using a SQUID magnetometer (Quantum Design MPMS-XL), applying a magnetic field of 0.1 T. All data were corrected for the contribution of the sample holder and the diamagnetism of the samples estimated from Pascal's constants.[38, 39] The magnetization measurements up to 5 T at 2-5 K. *ac* magnetic susceptibility was measured between 2 and 10 K with an oscillating field magnitude of 3.0 Oe and frequency ranging between 1 and 1488 Hz. The relaxation times were extracted from simultaneous fit of χ'_{ac} and χ''_{ac} using generalized Debye model.[40-44]

Antimicrobial Studies: The *in vitro* antibacterial efficacy of the oxazolidine ligand; H_3L_2 and its complexes with different transition metals, including four mononuclear complexes of Mn^{II}(**1**), Co^{II}(**2**), Ni^{II}(**3**), Zn^{II}(**4**), a tetranuclear iron (Fe^{III}_4) complex (**5**) and a trinuclear cobalt ($Co^{II}Co^{III}_2$) complex (**6**), were tested against both gram-positive and gram-negative

bacteria and in particular against the *Staphylococcus (S.) aureus* (NCTC 6571) *and Escherichia (E.) coli* (NCCTC 12923) *strains.* Most of the complexes were insoluble in common solvents including water, therefore, the antimicrobial activities of **1–6** complexes and that of the free ligand H_3L_2 were screened using the agar diffusion method.[45]

The bacterial strains used in this study were stored at -70 °C. Both strains were sub-cultured on Tryptic Soya Agar (TSA) before testing. The inoculum to be tested was prepared by adjusting the turbidity of an overnight culture in water to an optical density at 550 nm equivalent to $5x10^8$ Colony Forming Units (CFUs)/mL, according to the McFarland standard, and spread on Müller-Hinton agar. Subsequently the Müller-Hinton agar plates were inoculated and the antimicrobial activity of 0.5 mg of each compound was examined after overnight incubation at 37 °C. The antimicrobial activity of each compound was quantified by measuring the zone of inhibition in triplicate.

Synthetic procedures

$[M^{II}Cl(H_2L_2)(CH_3OH)]$ (M = Mn, Co, Ni for 1, 2, and 3, respectively) and $[Zn^{II}Cl(H_2L_2)]$ (4): 8-Hydroxyquinoline-2-carboxaldehyde (0.086 g, 0.5 mmol) and tris(hydroxymethyl)aminomethane (0.060 g, 0.5 mmol) were added to 20 mL of methanol and refluxed for 10 minutes. To the resulting yellow solution 2 mmol of the respective metal(II) chloride hexahydrate was added and refluxed for another 20 minutes. The resulting solution was filtered while still hot in a glass vial and left to evaporate slowly at room temperature (approximately 20 °C). After a few days, crystalline products formed with yields of 24% for $[Mn^{II}Cl(H_2L_2)(CH_3OH)]$ (**1**), 42% for $[Co^{II}Cl(H_2L_2)(CH_3OH)]$ (**2**), 22% for $[Ni^{II}Cl(H_2L_2)(CH_3OH)]$ (**3**), and 26% for $[Zn^{II}Cl(H_2L_2)]$ (**4**) with respect to 8-Hydroxy-2-quinolinecarboxaldehyde. **Elemental analyses;** calc. (exp): (**1**)**:** C, 45.30 (44.56); H, 4.82 (3.97); N, 7.04 (6.56). (**2**): C, 44.85 (43.97); H, 4.77 (4.03); N, 6.97(6.22). (**3**): C, 44.88(44.07); H, 4.77 (4.49); N, 6.98 (7.23). (**4**): C, 44.71 (43.87); H, 4.02 (4.21); N, 7.45 (6.34). **IR** (neat, cm^{-1}): **(1)** 3182 (m), 2948 (w), 2888 (w), 1570 (m), 1499 (m), 1450 (s), 1383 (m), 1329 (m), 1265 (m), 1191 (w), 1137 (w), 1074 (s), 1006 (s), 922 (m), 843 (s), 803 (w), 742 (m), 690 (w); **(2)** 3173 (m), 2952 (w), 2888 (w), 1573 (m), 1499 (m), 1449 (s), 1388 (m), 1332 (m), 1265 (s), 1190 (w), 1136 (w), 1079 (s), 1005 (s), 959 (w), 927 (m), 842 (s), 745 (s), 690 (w); **(3)** 3176 (m), 2950 (w), 2888 (w), 1576 (m), 1500 (m), 1448 (s), 1390 (m), 1330 (m), 1265 (s), 1193 (w), 1137 (w), 1078 (s), 1003 (s), 959 (w), 933 (m), 902 (w), 842 (s), 750 (s), 690 (w); **(4)** 3194 (m), 2954 (w), 2889 (w), 1574 (m), 1500 (m), 11450 (s), 1388 (m), 1333 (m), 1266 (m), 1228 (w), 1189 (w), 1074 (s), 1007 (s), 955 (w), 925 (m), 896 (w), 843 (s), 746 (s), 690 (w);

$[Fe^{III}_4(O)(HL_2)_2(H_3L_3)_2](NO_3)_2\bullet(CH_3CN)_2$(5): 8-Hydroxyquinoline-2-carboxaldehyde (0.086 g, 0.5 mmol), tris(hydroxymethyl)aminomethane (0.060 g, 0.5 mmol) and sodium acetate trihydrate (0.068 g, 0.5 mmol) were added to a mixture of 10 mL of methanol and 10 mL of acetonitrile and refluxed for 10 minutes. To the resulting solution iron(III) nitrate nonahydrate (0.130 g, 0.32 mmol) was added and the solution was refluxed for another 15 minutes. The resulting dark solution was filtered hot and left at room temperature (20 °C) for slow evaporation. Black crystals formed in three days with 46% yield with respect to 8-Hydroxy-2-quinoliecarboxaldyhe. **Elemental analyses** for desolvated **5: calc. (exp):** C, 50.87(48.12); H, 4.06(6.37); N, 10.38(8.29). IR: **(5) IR** (neat, cm^{-1}): 3212 (b), 3076 (w), 2929 (w), 2879 (w), 1577 (m), 1504 (m), 1465 (s), 1393 (m), 1332 (m), 1268 (m), 1179 (w), 1083 (s), 1016 (m), 965 (w), 825 (m), 747 (s), 662 (w), 603 (m);

$[Co^{II}Co^{III}_2(HL_2)_2(\mu^1\text{-}N_3)_2(\mu^2\text{-}N_3)_2]$ (6): 8-Hydroxyquinoline-2-carboxaldehyde (0.043 g, 0.25 mmol) and tris(hydroxymethyl)aminomethane (0.030 g, 0.25 mmol) were added to 20 mL of methanol and refluxed for 10 minutes. To the resulting yellow solution cobalt nitrate hexahydrate (0.291 g, 1 mmol) and sodium azide (0.065 g, 1 mmol) were added and the solution was refluxed for another 30 minutes and filtered hot and left to cool. After a few days of slow evaporation at room temperature (approximately 20 °C), dark block shaped crystals formed with 42% yield with respect to 8-Hydroxy-2-quinoliecarboxaldyhe. **Elemental analyses;** calc. (exp): C, 37.64(36.89); H, 3.16(2.78); N, 25.08(24.14). **IR** (neat, cm^{-1}): **(6)** 3277 (w), 3067 (m), 2924 (w), 2864 (w), 2067 (s), 2025 (s), 1581 (m), 1598 (w), 1461 (s), 1397 (m), 1363 (m), 1283 (m), 1210 (m), 1178 (m), 1126 (s), 1030 (s), 970 (m), 846 (m), 768 (s), 683 (m).

Results and discussion

All six complexes were synthesized in one-pot reactions. The ligands were synthesized *in situ* during the course of the reactions by refluxing a methanolic solution of 8-hydroxyquinoline-2-carboxaldehyde and TRIS in equimolar ratio. To the resulting solution the metal salts were added (four equivalent) and refluxed further for 20 minutes. Slow evaporation of the filtered solutions at ambient condition yielded crystalline products of compounds **1**-**4** suitable for single-crystal X-ray measurements. For Compound **5** and **6** sodium acetate and sodium azide were added as co-ligands, respectively. All the compounds were synthesized in methanol except for Compound **5** which was synthesized in a mixture of methanol and acetonitrile (1:1).

Ligand: The condensation of HQC and TRIS did not produce the expected imine ligand H_4L_1, but further cyclized to form the oxazolidine ligand H_3L_2 as shown in Scheme 1. To check if the cyclization process requires the presence of the metal ions the synthesis of the ligand was carried out independently from the precursor amine and aldehyde in methanol under reflux condition and without addition of any metal salts. The resulting solution was dried under vacuum and the yellow product was characterized as H_3L_2 by IR, NMR, and ESI-MS (see S8, S15 and S17 in ESI). It proves that the presence of the metal ions is not a requirement for the cyclization process and formation of the oxazolidine ligand. However, any possible catalytic role of the metal ions is not ruled out and was not studied during this investigation. This form of the ligand (H_3L_2) coordinates the metal ions with four donor atoms and present

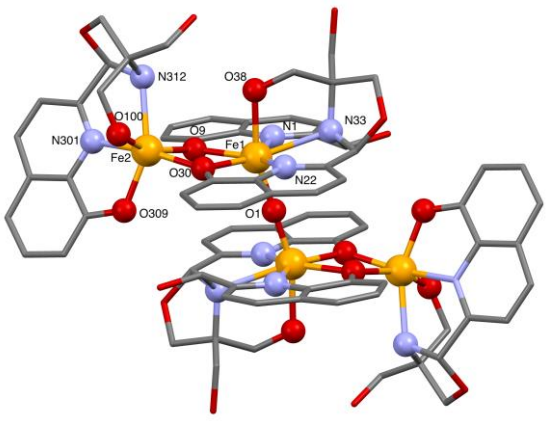

(A)

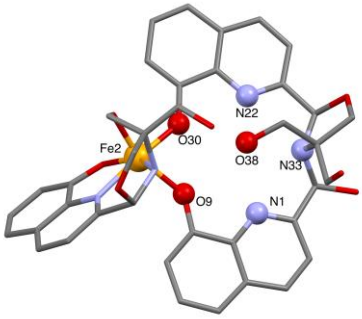

(B)

Figure 2. (A) The structure of tetranuclear iron complex as determined by single crystal X-ray crystallography. (B) The structure of metallamacrocycle acting as a five coordinate ligand to bind the central Fe(III) in Compound **5**. Colour code for the atoms: Blue (N), grey (C), red (O), orange (Fe).

in all six compounds (**1**-**6**). There is a second type of ligand that forms when H_3L_2 reacts with another equivalent of HQC to produce H_5L_3 (Scheme 2) with five coordinating groups on a plane. This ligand was found only in Compound **5**. This form of the ligand was also previously reported by Yan *et al.* in a series of mononuclear lanthanoid complexes.[36]

Structural description: Compounds **1** - **3** are isostructural and crystallize in monoclinic space group $P2_1/n$ with a molecular formula of $[M^{II}Cl(H_2L_2)(CH_3OH)]$ where M is Mn, Co, and Ni, for **1**, **2**, and **3**, respectively. Molecular structure of Compound **1** is shown in Figure 1A. The oxazolidine ligand (H_3L_2) satisfies four coordination sites of the metal ion, and three of the coordination bonds are through O1, N1, and N2 on the equatorial plane and the fourth alcoholic oxygen (O3) coordinates at the axial position. A chloride ion (Cl1) coordinates to the metal ion in the *trans* position to this alcoholic group, and a methanol satisfies the fourth coordination site (through O2) on the equatorial plane. It is worthnoting that there are two different kinds of hydroxyl groups in H_3L_2 and only the phenolic hydroxyl group is deprotonated. This can be easily explained by the higher acidity of phenolic groups compared to the primary alcohols due to the extra stability of the deprotonated form of phenolic hydroxyl groups gained through resonance. The bond

Table 1. Selected bond lengths between the metal (Atom 1) and the coordinating atoms (Atom 2) are given for compounds **1** – **4**

Atom 1	Atom 2	(**1**) Length/Å	(**2**) Length/Å	(**3**) Length/Å	(**4**) Length/Å
M1	Cl1	2.4550(5)	2.4149(5)	2.3884(5)	2.2450(5)
M1	O1	2.195(1)	2.119(1)	2.107(1)	2.071(1)
M1	O2	2.142(1)	2.053(1)	2.047(1)	-
M1	O3	2.269(1)	2.171(1)	2.113(1)	2.002(1)
M1	N1	2.181(1)	2.047(1)	1.979(1)	2.039(2)
M1	N2	2.347(1)	2.210(1)	2.167(1)	2.273(2)

distances between the metal ion and the coordinating atoms are given in Table 1.

It can be clearly seen that the six coordination bonds are uneven in lengths and the resulting geometry around the metal centres can be best described as slightly distorted octahedra. As a general trend the M-L bond distance decreases from Compound **1** to Compound **3** as can be seen from Table 1. Each molecule is bonded to six neighbouring molecules by inter-molecular hydrogen bonding, as shown in Figure S1 (see ESI). This extensive hydrogen bond networks assemble the molecules in a two-dimensional network, as shown in Figure S1. Compound **4** crystallizes in monoclinic space group $P2_1/c$ with a molecular formula of $[M^{II}Cl(H_2L_2)]$. Unlike compounds **1**-**3**, Compound **4** does not have the octahedral six coordinate geometry around Zn(II) ion. The coordination geometry of Zn(II) can be best described as distorted square pyramidal. The lack of preference to form octahedral complex for Compound **4** is possibly due to no additional gain of crystal field stabilization energy (CFSE) for the d^{10} electronic configuration of Zn(II) ion. The tetranuclear iron compound, $[Fe^{III}{}_4(O)(H_2L_2)_2(H_3L_3)_2]$ $(NO_3)_2$ $(CH_3CN)_2$ (**5**) was synthesized from a one-pot reaction from 8-Hydroxyquinoline-2-carboxaldehyde, tris(hydroxymethyl)aminomethane, sodium acetate trihydrate, and iron(III) nitrate nonahydrate in a 1:1 mixture of methanol and acetonitrile. Compound **5** crystallizes in triclinic space group *P-1*. The compound has two different types of ligands, one being the H_3L_2 similar to compounds **1**–**4**, and another form (H_4L_3) that forms from the condensation between H_3L_2 and 8- hydrxyquinoline-2-carboxaldehyde unit as shown in Scheme 2. There are two different kinds of iron (III) centres in the asymmetric unit of this compound, one is six-coordinate (Fe2) and the other is seven-coordinate (Fe1). The coordination geometry for Fe2 is highly distorted octahedron as can be seen from Figure 2A. The structure can be best described by assuming Fe1 coordinated to a metallamacrocycle formed by Fe2 and one H_3L_2 and one H_4L_3

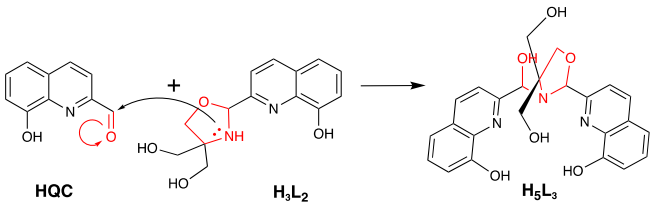

Scheme 2. Scheme showing the proposed pathway for the formation of H_5L_3. Red part is showing the atoms and bonds participating in the cyclization process.

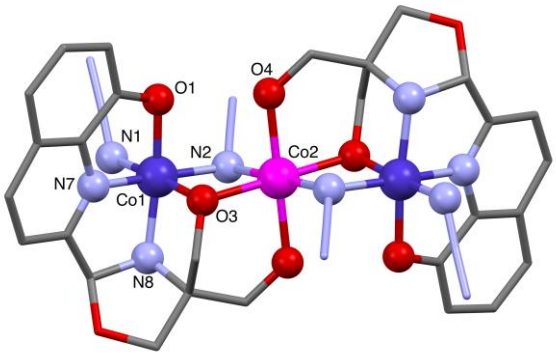

Figure 3. The structure of Compound **6** as determined by single crystal X-ray crystallography is shown. Colour code for the atoms: Blue (N), grey (C), red (O), magenta (Co^{II}), and dark-blue (Co^{III}).

as shown in Figure 2B. Two asymmetric units are linked *via* a linear μ^2-oxo bridge (O1) as shown in Figure 2B. The Fe1 is coordinate to the five atoms of the metallamacrocycles, and Fe1 shares a plane with four coordinating atoms (N1N22O30O9) leaving N33 slightly above the plane. All the angles are listed in Table S5 in the ESI. Each molecule of Compound **5** is connected to the neighbouring molecules through hydrogen bonding and results into a porous three-dimensional structure, with 5.9 % solvent accessible pore volume for a probe of 1.2 Å radius, as shown in Figure S2B in the ESI.[46]

Reaction between 8-Hydroxyquinoline-2-carboxaldehyde, tris(hydroxymethyl)aminomethane, sodium azide, and cobalt nitrate hexahydrate produced a trinuclear cobalt complex, $[Co^{II}Co^{III}_2(HL_2)_2(\eta^1\text{-}N_3)_2(\mu^2\text{-}1,1\text{-}N_3)_2]$ **(6)** (Figure 3). Compound **6** crystallizes in a monoclinic space group $P2_1/c$ with an asymmetric unit containing two cobalt atoms with different oxidation states, Co^{III}, and Co^{II}, respectively. Unlike the previous compounds (**1**-**5**), in compound **6** the ligand H_3L_2 coordinates through all the available hydroxyl groups. The ligand coordinates to Co1 with five donor atoms and coordinates Co2 using one terminal hydroxy group and one deprotonated hydroxy group acts as a bridging group between Co1 and Co2. There are two different kinds of coordination for the azide groups in this complex, two terminal azide ligands coordinate to the two terminal Co1 metal centres, and two azides bridge between the central Co(II) and the terminal Co(III) atoms with μ^2-1,1-N_3 mode as as shown in Figure 3.[47] The coordination environment of the two types of cobalt atoms are very different. The terminal Co(III) centres have N4O2 coordination sphere, but the central Co(II) has a N2O4 coordination sphere. Its worthnoting that relatively longer Co2-N2 bonds might be a result of Jahn-Teller distortion expected for a d^7 low-spin configuration. The ∠Co1-N2-Co2 and ∠Co1-O3-Co2 angles are 93.49(9) and 97.96(7), respectively. Each molecule is weakly bonded to the two neighbouring molecules through hydrogen bonding between the terminal azide units and the N-H group of the oxazolidine ring to form an one-dimension chain, as shown in Figure S3 in ESI.

As a general observation it is worth noting that the mononuclear complexes formed only with +2 oxidation state of the first row transition metals (Mn, Co, Ni, and Zn), and polynuclear complexes were observed for metal ions with higher oxidation states and in presence of other co-ligands in this current study.

Thermal stability: The thermal stability of all the compounds were tested using thermogravimentric analysis (TGA) and compound **1**-**3** shows a similar trend with three step decomposition with loss of the coordinate methanol molecule around approximately 200 °C at the first step, followed by another step around 275 °C which accounts the loss of one HCl molecule (for **2**, observed loss: 9.40%, calculated: 8.90%), and the final decomposition around 400 °C without a distinct decomposition temperature. The residual mass is very close to the expected mass for the metal oxide. For example, for compound **2**, the observed residual mass is 18.16 %, which is very close to the calculated mass of 18.65% for $Co^{II}O$. Compound **5** shows approximately 4% mass loss around 75 °C possibly due to loss of lattice solvents (CH_3CN) followed by another step-like decomposition around 150 °C followed by a gradual final decomposition starting around 250 °C to result into a residual mass of 18.84%. Compound **6** has an intermediate mass loss around 165 °C possibly due to the decomposition of the azide groups followed by a final decomposition at around 350 °C to form Co_3O_4 with an observed residual mass of 25.10% (calculated 26.95%).

Infrared Spectroscopy: The IR spectra (see Figures S4-S7 in ESI) of compound **1** to **4** display a medium, sharp peak located at 3182, 3173, 3176 and 3194 cm^{-1} for **1**, **2**, **3**, and **4**, respectively, indicative of N-H stretching, caused by the nitrogen coordinating with the metal ions. This band overlays a weaker, broad (3500 cm^{-1} to 3200 cm^{-1}) peak, indicative of alcohol O-H stretching and interactions due to hydrogen bonding. Compound **5** displays a weak, broad O-H stretching band at 3212 cm^{-1}, whereas a weak, aromatic sp^2 peak can be found at 3076 cm^{-1}. The two weak peaks present at roughly 2950 and 2888 cm^{-1} in all five spectra are an indication of sp^3 hybridized alkane C-H stretching. The medium, sharp peak present near 1570 cm^{-1} on all five spectra can be identified as C=C aromatic stretching, along with the strong peak around 1450 cm^{-1}, which can be attributed to aromatic C-C stretching. The medium, sharp peak between 1380 cm^{-1} and 1393 cm^{-1} can be interpreted as alkane C-H bending. The medium, sharp band found near 1330 cm^{-1} is indicative of C-N stretching, and the strong, sharp band present near 1070 cm^{-1} (1083 cm^{-1} in case of **5**) can be ascribed to alcohol C-O stretching. For Compound **6**, the peak at 3277 cm^{-1} (w) is indicative of N-H stretching of a secondary amine. The band at 3067 cm^{-1} (m) indicates unsaturated sp^2 hybridized C-H stretching, while the two weak saturated sp^3 C-H stretching. The two strong, sharp peaks 2067 cm^{-1} and 2025 cm^{-1} originating from the presence of N-N triple bonds of the terminal and bridging azide groups, respectively. The medium band at 1581 cm^{-1} and the strong band at 1461 cm^{-1} can be attributed to aromatic C=C and C-C stretching respectively. The medium band at 1283 cm^{-1} indicates C-N

stretching, and the strong band at 1030 cm^{-1} can be assigned to the alcoholic C-O stretching.

Electrospray ionization Mass Spectroscopy (ESI-MS): The isolated ligand (H_3L_2) and all six compounds (**1**-**6**) were analysed by ESI-MS (Figure S17 –S23 in ESI). The presence of the corresponding $^{m}/_{z}$ peaks suggests the existence of the singly charged entities (with $+H^+$ or $–Cl^-$) for the ligand, and the compounds **1** – 4. The presence of doubly charged $[Fe^{III}_4(O)(H_2L_2)_2(H_3L_3)_2]^{2+}$ species was detected for Compound **5**. However, the detection of any identifiable fragment for Compound **6** remained unsuccessful possibly due to the decomposition of the compound in solution or under ESI conditions.

NMR studies: Attempt was made to look into the mechanism of formation of the ligand and to check if the presence of the metal ions is a requirement for the cyclization process. The ligand solution was evaporated at reduced pressure prior to addition of any metal ions, and the crystalline yellowish solid was analysed by NMR spectroscopy, which clearly showed the peaks corresponding to the oxazolidine ligand (see Figure S15 in ESI), indicating that the presence of the metal ion is not a requirement for the cyclization process. However, any possible catalytic role of the metal ions is not excluded. The zinc complex (Compound **4**) was also analysed with NMR spectroscopy and the peaks corresponding to the oxazolidine were assigned as shown in the 2D NMR spectra shown in Figure 4.

Magnetic properties: The magnetic susceptibility measurements of compounds **5** and **6** were performed at variable temperature (2-300 K), at 0.1 T and the resulting $\chi_M T$ *vs* *T* plots are shown in Figure 5A. The magnetic susceptibility of Compound **5** is 9.32 $cm^3 \cdot K \cdot mol^{-1}$ at 300 K is much smaller compared to the expected value of 17.514 $cm^3 \cdot K \cdot mol^{-1}$ for four Fe^{III} ($^6A_{1g}$, S = 5/2, g = 2)[39] suggests strong antiferromagnetic interactions. Due to dominant antiferromagnetic interaction at 2 K the product of $\chi_M T$ have a value of 0.16 suggesting the ground spin state of S = 0. Based on the magnetostructural correlation the magnetic susceptibility data of **5** was analysed[48] using the following Hamiltonian:

$H = -2J_1(S_1S_2+S_3S_4)-2J_2S_2S_3$

The best fit between theoretical and experimental data was obtained for J_1 = -8.0 cm^{-1}, J_2 = -75.0 cm^{-1}, and g = 2.03. The large value of coupling constant (J_2) along μ-oxo bridge is consistent with similar cases previously reported on Fe^{III}-O-Fe^{III} geometry.[49]

The susceptibility plot for Compound **6** is presented in Figure 5B showing that the $\chi_M T$ value of 3.04 $cm^3 \cdot K \cdot mol^{-1}$ at 300 K, which is consistent with the presence of one isolated paramagnetic Co(II) centre. Upon decreasing temperature, the $\chi_M T$ product continuously decreases and reach the value of 2.00 $cm^3 \cdot K \cdot mol^{-1}$ at 2 K. Such temperature dependence of the magnetic susceptibility is typical for mononuclear Co(II)

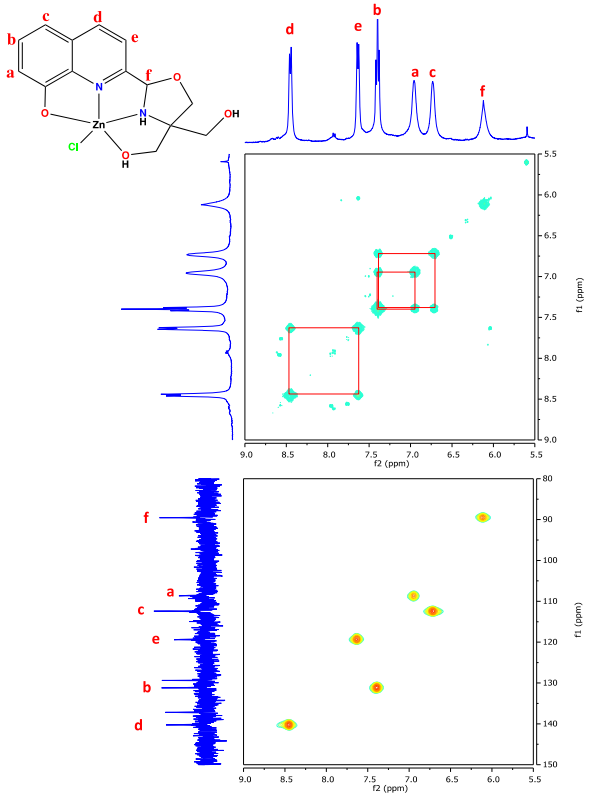

Figure 4. NMR spectra (400 MHz) of Compound **4** in DMSO-d_6 are shown: Selected area ^1H, ^1H COSY (top) and ^1H, ^{13}C HMBC spectrum (bottom).

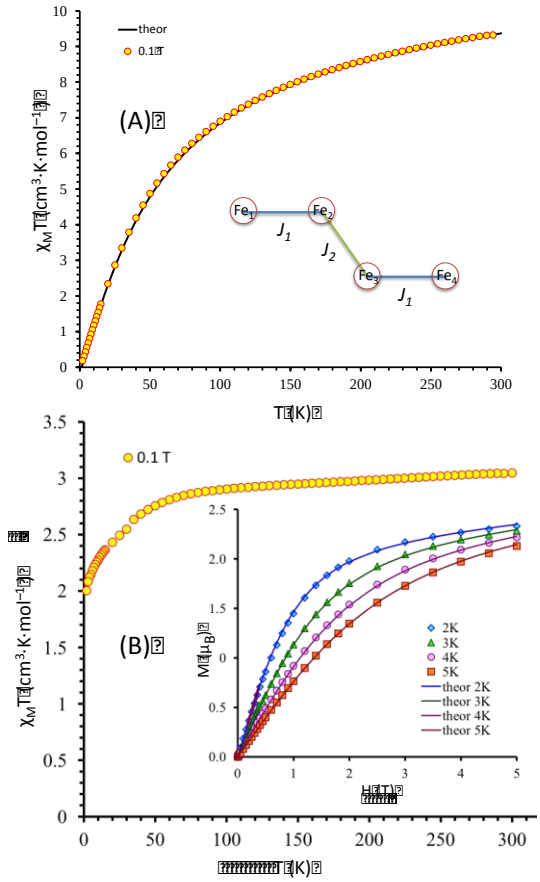

Figure 5. Temperature dependence of the χT product at H_{dc} = 0.1 T for Compound **5** (A) and **6** (B)**.** The solid line is simulated susceptibility according the model discussed in the text. Magnetization plot for Compound **6** is given (inset B) at different temperatures.

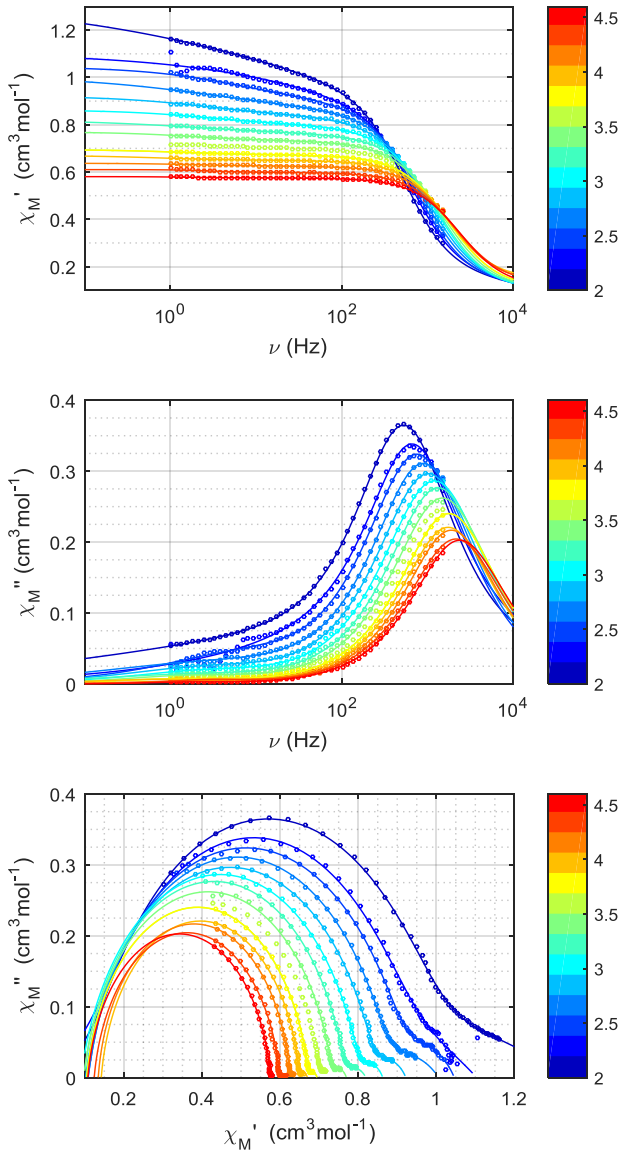

Figure 6. Frequency dependence of χ'_{ac} (top), χ''_{ac} (middle), and Cole-Cole plot (χ'_{ac} vs. χ''_{ac}) (bottom) are shown at different temperatures (2 – 4.5 K) for Compound **6**.

compounds and is related to presence of important magnetic anisotropy.[50-53]

To determine the anisotropy parameters the magnetization plot (Figure 5B, inset) was fitted using the following Hamiltonian: [54]

$$H = DS_z^2 + E\left(S_x^2 - S_y^2\right) + g\mu_B SB$$

Where *D*, *E* and *g* stand for the axial and rhombic zero-field splitting (ZFS) parameters and the isotropic Landé factor of the *S* spin state, μ_B and *B* stand for the Bohr magneton and magnetic field, respectively. The parameters obtained for best fit are *D* = - 25.65 cm^{-1} E = 3.42 cm^{-1} and *g* = 2.70 (R = 7.8×10^{-3}). Dynamic magnetic properties of the trinuclear cobalt complex (**6**) were investigated. At zero *dc* field, no out-of-phase (χ''_{ac}) signal was observed. Applying a small *dc* field of 2000 Oe a signal in χ''_{ac} can be detected. The *ac* data were fitted using an extended Debye model[42-44] for two relaxation processes (Figure 6). The model with one relaxation process does not give satisfactory fit. The presence of two relaxation process in several mononuclear Co(II) complexes have been previously observed.[55-59]

The analysis of temperature dependence of relaxation times at *dc* field of 2000 Oe reveal an energy barrier of slow magnetic relaxation of 5.1 K with τ_0 = 2*10^{-5} (see figure S24 in ESI) which is much smaller than the zero-field energy gap of magnitude 2D as predicted by the static magnetic measurements. This discrepancy excludes the Orbach relaxation process and suggests the direct spin phonon relaxation or Raman mechanism of relaxation in **6**.[60-62]

Antimicrobial studies:

Bacterial resistance development has become a serious clinical problem for many classes of antibiotics. Oxazolidinones are a unique class of synthetic antibiotics, that are active mainly against Gram-positive organisms, but they also display modest activity against certain gram negative. The effect of the presence of the ligand H_3L_2 and all six complexes (**1**-**6**) on the bacterial growth on the Müller-Hinton agar plates is shown in Figure S25 in the ESI. The antibacterial activity of the ligand and its complexes against *S. aureus* and *E. coli* is presented as zone of inhibition in mm, and the results are given in Table 2.

It can be clearly seen that the oxazolidine ligand (H_3L_2) shows substantial antimicrobial activity against both bacterial strains. Compounds **1**-**4** show antimicrobial activity but this is reduced in comparison to the ligand and this depends on the metal and the complex that has been formed. In particular, Compound **1**, followed by Compound **4** show better antimicrobial efficacy against *S. aureus* than *E. coli*. Complexes **2** and **3** show comparable activity against both *S. aureus* and *E. coli* but this is significantly reduced in comparison to the ligand and the compounds **1** and **4**. Compounds **5** and **6** do not show any antimicrobial activity against either of the strains. Oxazolidinones are well known for their efficacy against Gram-positive bacteria.[63] The produced oxazolidine (ligand) of this study showed good antimicrobial activity not only against Gram-positive bacteria but against Gram-negative too. The antimicrobial efficacy testing of metal (Mn, Fe, Co, Ni, Cu) chelates of 1, 2-naphthoquinone 2-oxime has shown that Mn complex is more potent than Cu complex and these two are more potent than Co and Ni complexes, in an order that agrees with the finding of Jadav *et al.*,[64] while the iron(III) complex did not show any activity against Gram-positive bacteria but did against Gram-negative bacteria. The results indicate that the antimicrobial properties are possibly originating from the ligand H_3L_2 only, and persist in presence of M^{2+} ions. However, the antimicrobial properties are lost when the ligand is coordinate to metal ions with higher oxidation state (+3 here). One possible explanation may be due to less availability of the free ligands due to stronger

Table 2. Zones of inhibition in mm of ligand H_3L_2 and its complexes; 1 – 6

Compound	H_3L_2	(1)	(2)	(3)	(4)	(5)	(6)
S. aureus	34±1.6	23.3±1.3	13.3±0.5	3.7±0.5	18±0.8	0±0	0±0
E. coli	20.3±0.5	5±0.8	11.7±0.5	6.7±0.5	11.3±0.9	0±0	0±0

binding with the higher oxidation state metal ions.

Conclusions

In summary, a new oxazolidine based ligand H_3L_2 has been synthesized by *in situ* cyclization, and its four mononuclear complexes of Mn^{II}, Co^{II}, Ni^{II}, and Zn^{II}, a tetranuclear Fe^{III}_4 complex, and a trinuclear Co^{III}-Co^{II}-Co^{III} complex (Compound **1**-**6**, respectively) have been synthesized. Magnetic properties of the polynuclear complexes (**5**, and **6**) have been studied in detail. The dominant antiferromagnetic interaction was found in the case of Compound **5** (J_1 = -8.0 cm^{-1} J_2 = -75.0 cm^{-1} g = 2.03). Compound **6** has behaviour typical for isolated paramagnetic Co^{II} centre in octahedral environment and show slow relaxation of magnetisation at 2 K. The oxazolidine ligand (H_3L_2) of this study showed good antimicrobial activity not only against Gram-positive bacteria but also against Gram-negative bacteria. The antimicrobial efficacy of the metal complexes (**1**-**6**) is also reported.

Conflicts of interest

There are no conflicts to declare.

Acknowledgements

SN thanks Royal Society of Chemistry for a Research Fund award, and University of Bradford for research facilities. A fruitful discussion with Dr Małgorzata Hołyńska is kindly acknowledged.

Notes and references

1 A. M. Ako, I. J. Hewitt, V. Mereacre, R. Clerac, W. Wernsdorfer, C. E. Anson and A. K. Powell, *Angew. Chem., Int. Ed.*, 2006, **45**, 4926-4929.
2 L. Bogani and W. Wernsdorfer, *Nat. Mater.*, 2008, **7**, 179-186.
3 C. J. Milios, A. Vinslava, W. Wernsdorfer, S. Moggach, S. Parsons, S. P. Perlepes, G. Christou and E. K. Brechin, *J. Am. Chem. Soc.*, 2007, **129**, 2754-2755.
4 J. S. Kanady, E. Y. Tsui, M. W. Day and T. Agapie, *Science*, 2011, **333**, 733-736.
5 E. E. Moushi, T. C. Stamatatos, W. Wernsdorfer, V. Nastopoulos, G. Christou and A. J. Tasiopoulos, *Inorg. Chem.*, 2009, **48**, 5049-5051.
6 M. Murugesu, J. Raftery, W. Wernsdorfer, G. Christou and E. K. Brechin, *Inorg. Chem.*, 2004, **43**, 4203-4209.
7 S. Nayak, G. aromi, S. J. Teat, J. R. Ariño, P. Gamez and J. Reedijk, *Dalton Trans.*, 2010, **39**, 4986-4990.
8 S. Nayak, L. M. C. Beltran, Y. Lan, R. Clérac, N. G. R. Hearns, W. Wernsdorfer, C. E. Anson and A. K. Powell, *Dalton Trans.*, 2009, 1901-1903.
9 Y. Xie, H. Jiang, A. S.-C. Chan, Q. Liu, X. Xu, C. Du and Y. Zhu, *Inorg. Chim. Acta*, 2002, **333**, 138-143.
10 Y. Xie, W. Bu, A. S.-C. Chan, X. Xu, Q. Liu, Z. Zhang, J. Yu and Y. Fan, *Inorg. Chim. Acta*, 2000, **310**, 257-260.
11 Y. Xie, J. Ni, F. Zheng, Y. Cui, Q. Wang, S. W. Ng and W. Zhu, *Cryst. Growth Des.*, 2009, **9**, 118-126.
12 S. Nayak, A. Pevec, C. C. Seaton, P. Gamez and J. Reedijk, *Polyhedron*, 2016, **107**, 172-175.
13 S. Nayak, H. P. Nayek, S. Dehnen, A. K. Powell and J. Reedijk, *Dalton Trans.*, 2011, **40**, 2699-2702.
14 Y. Lan, G. Novitchi, R. Clerac, J. K. Tang, N. T. Madhu, I. J. Hewitt, C. E. Anson, S. Brooker and A. K. Powell, *Dalton Trans.*, 2009, **0**, 1721-1727.
15 H. Miyasaka, R. Clerac, T. Ishii, H. C. Chang, S. Kitagawa and M. Yamashita, *J. Chem. Soc.-Dalton Trans.*, 2002, **0**, 1528-1534.
16 Z. Lü, M. Yuan, F. Pan, S. Gao, D. Zhang and D. Zhu, *Inorg. Chem.*, 2006, **45**, 3538-3548.
17 D. Dragancea, N. Talmaci, S. Shova, G. Novitchi, D. Darvasiová, P. Rapta, M. Breza, M. Galanski, J. Kožíšek, N. M. R. Martins, L. M. D. R. S. Martins, A. J. L. Pombeiro and V. B. Arion, *Inorg. Chem.*, 2016, **55**, 9187-9203.
18 L.-L. Hu, Z.-Q. Jia, J. Tao, R.-B. Huang and L.-S. Zheng, *Dalton Trans.*, 2008, **0**, 6113-6116.
19 Z.-Q. Jia, X.-J. Sun, L.-L. Hu, J. Tao, R.-B. Huang and L.-S. Zheng, *Dalton Trans.*, 2009, **0**, 6364-6367.
20 C. Ding, C. Gao, S. Ng, B. Wang and Y. Xie, *Che. Eur. J.*, 2013, **19**, 9961-9972.
21 C.-X. Ding, J. Ni, Y.-H. Yang, S.-W. Ng, B.-W. Wang and Y.-S. Xie, *Crystengcomm*, 2012, **14**, 7312-7319.
22 S. Nayak, G. Novitchi, S. Muche, D. Luneau and S. Dehnen, *Z. Aorg. Allg. Chem.* , 2012, **638**, 1127-1133.
23 S. Nayak, O. Roubeau, S. Teat, C. Beavers, P. Gamez and J. Reedijk, 2010, **49**, 216-221.
24 E. D. Bergmann, *Chem. Rev.*, 1953, **53**, 309-352.
25 S. Gandhi, A. Bisai, B. A. B. Prasad and V. K. Singh, 2007, **72**, 2133-2142.
26 C. Agami and F. Couty, *Eur. J. Org. Chem.*, 2004, **2004**, 677-685.
27 C. W. Ford, J. C. Hamel, D. M. Wilson, J. K. Moerman, D. Stapert, R. J. Yancey Jr, D. K. Hutchinson, M. R. Barbachyn and S. J. Brickner, *Antimicrob. Agents Chemother.*, 1996, **40**, 1508-1513.
28 E. A. Swinyard, W. C. Brown and L. S. Goodman, *J. Pharm. Exp. Ther.*, 1952, **106**, 319-330.
29 G. Desimoni, G. Faita and K. A. Jørgensen, *Chem. Rev.*, 2006, **106**, 3561-3651.
30 L. M. Geary and P. G. Hultin, *Tetrahedron*, 2009, **20**, 131-173.
31 G. A. Ardizzoia, S. Brenna and B. Therrien, *Dalton Trans.*, 2012, **41**, 783-790.
32 R. W. Saalfrank, H. Maid, F. Hampel and K. Peters, *Eur. J. Inorg. Chem.*, 1999, **1999**, 1859-1867.
33 C. Ding, F. Zeng, J. Ni, B. Wang and Y. Xie, *Cryst. Growth Des.*, 2012, **12**, 2089-2096.
34 C. Wolf and H. Xu, *Chem. Commun.*, 2011, **47**, 3339-3350.
35 F. Duan, L. Liu, C. Qiao and H. Yang, *Inorg. Chem. Commun.*, 2015, **55**, 120-122.
36 M. Zhang, H. Li, P. Chen, W. Sun, L. Zhang and P. Yan, *J. Mol. Str.*, 2015, **1081**, 233-236.
37 G. M. Sheldrick, *Acta Crystallogr. Sect. A*, 2008, **64**, 112-122.
38 P. Pascal, *Ann. Chim. Phys.*, 1910, **19**, 5-13.
39 O. Kahn, *Molecular Magnetism*, Wiley-VCH, 1993.
40 C. Dekker, A. F. M. Arts, H. W. Wijn, A. J. van Duyneveldt and J. A. Mydosh, *Phys. Rev. B.*, 1989, **40**, 11243-11251.
41 K. S. Cole and R. H. Cole, *J. Chem. Phys.*, 1941, **9**, 341-351.
42 Y.-N. Guo, G.-F. Xu, Y. Guo and J. Tang, *Dalton Trans.*, 2011, **40**, 9953-9963.
43 Y. N. Guo, G. F. Xu, W. Wernsdorfer, L. Ungur, Y. Guo, J. K. Tang, H. J. Zhang, L. F. Chibotaru and A. K. Powell, *J. Am. Chem. Soc.*, 2011, **133**, 11948-11951.
44 Y.-N. Guo, G.-F. Xu, P. Gamez, L. Zhao, S.-Y. Lin, R. Deng, J. Tang and H.-J. Zhang, *J. Am. Chem. Soc.*, 2010, **132**, 8538-8539.
45 J. Han, M. E. Castell-Perez and R. G. Moreira, *WT-Food Sci. Technol.*, 2007, **40**, 1545-1554.
46 C. F. Macrae, I. J. Bruno, J. A. Chisholm, P. R. Edgington, P. McCabe, E. Pidcock, L. Rodriguez-Monge, R. Taylor, J. van de Streek and P. A. Wood, *J. Appl. Crystallogr.*, 2008, **41**, 466-470.

47 Y.-F. Zeng, X. Hu, F.-C. Liu and X.-H. Bu, *Chem. Soc. Rev.*, 2009, **38**, 469-480.
48 J. J. Borras-Almenar, J. M. Clemente-Juan, E. Coronado and B. S. Tsukerblat, *J. Comp. Chem.*, 2001, **22**, 985-991.
49 S. M. Gorun and S. J. Lippard, *Inorg. Chem.*, 1991, **30**, 1625-1630.
50 J. Titiš and R. Boča, *Inorg. Chem.*, 2011, **50**, 11838-11845.
51 J. Titiš, J. Hudák, J. Kožíšek, A. Krutošíková, J. Moncol', D. Tarabová and R. Boča, *Inorg. Chim. Acta.*, 2012, **388**, 106-113.
52 B. Papánková, R. Boča, Ľ. Dlháň, I. Nemec, J. Titiš, I. Svoboda and H. Fuess, *Inorg. Chim. Acta.*, 2010, **363**, 147-156.
53 C. Rajnák, J. Titiš, R. Boča, J. Moncol' and Z. Padělková, *Monatsh. Chem.*, 2011, **142**, 789-795.
54 M. P. Shores, J. J. Sokol and J. R. Long, *J. Am. Chem. Soc.*, 2002, **124**, 2279-2292.
55 E. A. Buvaylo, V. N. Kokozay, O. Y. Vassilyeva, B. W. Skelton, A. Ozarowski, J. Titiš, B. Vranovičová and R. Boča, *Inorg. Chem.*, 2017, **56**, 6999-7009.
56 C. Rajnak, F. Varga, J. Titis, J. Moncol and R. Boca, *Eur. J. Inorg. Chem.*, 2017, 1915-1922.
57 C. Rajnak, J. Titis, O. Fuhr, M. Ruben and R. Boca, *Inorg. Chem.*, 2014, **53**, 8200-8202.
58 A. V. Palii, D. V. Korchagin, E. A. Yureva, A. V. Akimov, E. Y. Misochko, G. V. Shilov, A. D. Talantsev, R. B. Morgunov, S. M. Aldoshin and B. S. Tsukerblat, *Inorg. Chem.*, 2016, **55**, 9696-9706.
59 R. Boca, J. Miklovic and J. Titis, *Inorg. Chem.*, 2014, **53**, 2367-2369.
60 Y.-Z. Zhang, S. Gomez-Coca, A. J. Brown, M. R. Saber, X. Zhang and K. R. Dunbar, *Chem. Sci.*, 2016, **7**, 6519-6527.
61 V. V. Novikov, A. A. Pavlov, Y. V. Nelyubina, M.-E. Boulon, O. A. Varzatskii, Y. Z. Voloshin and R. E. P. Winpenny, *J. Am. Chem. Soc.*,, 2015, **137**, 9792-9795.
62 E. Colacio, J. Ruiz, E. Ruiz, E. Cremades, J. Krzystek, S. Carretta, J. Cano, T. Guidi, W. Wernsdorfer and E. K. Brechin, *Angew. Chem. Int. Ed.*, 2013, **52**, 9130-9134.
63 M. F. Gordeev and Z. Y. Yuan, *J. Med. Chem.*, 2014, **57**, 4487-4497.
64 V. B. Jadhav, H. P. Desimukh, N. R. Gonewar, K. D. Jadhav and R. G. Sarawadekar, *Int. J. Chem. Sci.*, 2013, **11**, 1286-1298.

Journal Name

ARTICLE

Table 3. Crystallographic data for compounds **1 – 6.**

Compound	1	2	3	4	5	6
CCDC reference no.	1832155	1832156	1832157	1832158	1588548	1832159
Empirical formula	$C_{15}H_{19}ClMnN_2O_5$	$C_{15}H_{19}ClCoN_2O_5$	$C_{15}H_{19}ClN_2NiO_5$	$C_{14}H_{15}ClN_2O_4Zn$	$C_{80}H_{76}Fe_4N_{14}O_{27}$	$C_{28}H_{28}Co_3N_{16}O_8$
Formula weight	397.71	401.70	401.48	376.10	1888.94	893.45
Temperature/K	100(2)	100(2)	100(2)	100(2)	173(2)	100(2)
Crystal system	monoclinic	monoclinic	monoclinic	monoclinic	triclinic	monoclinic
Space group	$P2_1/n$	$P2_1/n$	$P2_1/n$	$P2_1/c$	P-1	$P2_1/c$
a/Å	13.1683(5)	13.1024(5)	13.0791(5)	11.0694(5)	11.9096(6)	9.4740(4)
b/Å	8.5529(3)	8.5218(3)	8.4696(3)	9.1258(4)	12.5269(7)	17.7982(6)
c/Å	14.3906(6)	14.1371(6)	14.1012(5)	13.8053(6)	17.0352(10)	9.7057(4)
α/°	90	90	90	90	83.424(4)	90
β/°	91.695(2)	90.3820(10)	90.0920(10)	91.676(2)	81.197(5)	97.4270(10)
γ/°	90	90	90	90	69.805(4)	90
Volume/$Å^3$	1620.06(11)	1578.46(11)	1562.05(10)	1393.98(11)	2351.9(2)	1622.85(11)
Z	4	4	4	4	1	2
$\rho_{calc}g/cm^3$	1.631	1.690	1.707	1.792	1.334	1.828
μ/mm^{-1}	1.008	1.286	1.443	1.974	5.522	1.595
F(000)	820.0	828.0	832.0	768.0	974.0	906.0
Crystal size/mm^3	0.380 × 0.170 × 0.160	0.271 × 0.138 × 0.102	0.140 × 0.140 × 0.080	0.340 × 0.082 × 0.032	0.65 × 0.34 × 0.32	0.16 × 0.12 × 0.11
Radiation	MoKα (λ = 0.71073)	MoKα (λ = 0.71073)	MoKα (λ = 0.71073)	MoKα (λ = 0.71073)	CuKα (λ = 1.54184)	MoKα (λ = 0.71073)
2Θ range for data collection/°	5.542 to 55.062	5.582 to 55.024	4.25 to 55.05	5.352 to 55.046	5.262 to 134.142	4.812 to 52.814
Index ranges	$-17 \le h \le 17$, $-10 \le k \le 11$, $-18 \le l \le 18$	$-17 \le h \le 17$, $-9 \le k \le 11$, $-18 \le l \le 18$	$-16 \le h \le 16$, $-11 \le k \le 11$, $-18 \le l \le 18$	$-14 \le h \le 14$, $-11 \le k \le 10$, $-17 \le l \le 17$	$-14 \le h \le 13$, $-14 \le k \le 14$, $-20 \le l \le 18$	$-11 \le h \le 11$, $-22 \le k \le 21$, $-12 \le l \le 12$
Reflections collected	20227	16727	20426	17433	10875	21623
Independent reflections	3715 [R_{int} = 0.0337, R_{sigma} = 0.0246]	3618 [R_{int} = 0.0274, R_{sigma} = 0.0232]	3590 [R_{int} = 0.0253, R_{sigma} = 0.0201]	3200 [R_{int} = 0.0362, R_{sigma} = 0.0268]	7709 [R_{int} = 0.0619, R_{sigma} = 0.1347]	3319 [R_{int} = 0.0482, R_{sigma} = 0.0299]
Data/restraints/parameters	3715/1/235	3618/0/235	3590/0/235	3200/0/211	7709/895/727	3319/58/276
Goodness-of-fit on F^2	1.034	1.055	1.077	1.038	0.974	1.024
Final R indexes [I>=2σ (I)]	R_1 = 0.0291, wR_2 = 0.0660	R_1 = 0.0286, wR_2 = 0.0649	R_1 = 0.0283, wR_2 = 0.0645	R_1 = 0.0267, wR_2 = 0.0589	R_1 = 0.0702, wR_2 = 0.1676	R_1 = 0.0335, wR_2 = 0.0791
Final R indexes [all data]	R_1 = 0.0379, wR_2 = 0.0696	R_1 = 0.0363, wR_2 = 0.0682	R_1 = 0.0330, wR_2 = 0.0667	R_1 = 0.0354, wR_2 = 0.0623	R_1 = 0.1071, wR_2 = 0.1813	R_1 = 0.0466, wR_2 = 0.0851
Largest diff. peak/hole / e $Å^{-3}$	0.42/-0.36	0.45/-0.41	0.49/-0.39	0.69/-0.43	0.68/-0.92	0.57/-0.46